Theor Chim Acta (1995) 91: 199–214

Theoretica Chimica Acta

Solvent effects on isomerization equilibria: an energetic analysis in the framework of density functional theory

Francesco Lelj, Carlo Adamo

Dipartimento di Chimica, Università della Basilicata, via N. Sauro 85, I-85100 Potenza, Italy; e-mail: LEL J@ pzvx85.CINECA.IT

Received April 14, 1994/Final revision received August 3, 1994/Accepted October 11, 1994

Summary. We have analyzed equilibrium solvent effects on some isomerization reactions, chosen as the most representative of this wide class of reaction in organic and inorganic chemistry. Solvent effects were modeled by the self-consistent reaction field approach, in the framework of the density functional computational scheme, as implemented in the ADF package. We have investigated as "organic reactions" the formamide/formamidic acid and 2-pyridone/2-hydroxypyridine tautomerization reactions, whereas the linkage isomerization of pentaamminenitro cobalt(II) to pentaamminenitrito cobalt(II) was chosen as representative of inorganic isomeric equilibria.

The three examples point out three different limiting behaviors deriving from the interplay of electrostatic and polarization contributions to the total energy.

Key words: Solvation – Density functional theory – Formamide – 2-Pyridone – Pentaamminenitro cobalt (II)

1 Introduction

Interactions between solute and solvent molecules are representative for variations of physical and chemical properties of the solute in going from the gas phase to the condensed phase (solution or solid state). They can also strongly influence the energetics of the solute reaction mechanisms and, sometimes, the reaction paths.

Problems involving static and dynamical aspects of solute–solvent interactions are often treated in the framework of the adiabatic approximation. In this approximation the evolution of the solute along the reaction path is accompanied by an averaged description of the solvent degrees of freedom, determined for each point of the solute reaction coordinate. This description corresponds to an equilibrium response model, based on the assumption that the solvent instantly adjusts itself to any variations of the solute coordinates. These solvent effects do not require the explicit inclusion of solvent degrees of freedom, that are fixed while the process occurs, in the reaction coordinate. As a consequence solvent molecules give only energetic contributions to the reaction without altering the reaction coordinate obtained for the same process in the gas phase. We can refer to these effects as equilibrium or static solvent effects. On the other hand, in a real system the solvent

molecules will require a finite time to relax from a state of equilibrium when a change in the solute coordinate space occurs. Moreover, specific solute–solvent interaction can take place, as occurs when atoms of the solvent molecules directly participate in the reaction mechanism. These solvent effects require a more dynamical treatment of the solvent coordinates and are called dynamic or non-equilibrium solvation effects [1–5]. There are in the literature several studies on dynamical solvent effects. They range from classical methods resting on Newton's equations of motion (such as the molecular mechanics methods) [6–9], in which several hundred solvent molecules are explicitly considered, to intermediate approaches in which the solute molecule is treated quantum mechanically and solvent molecules by classical mechanics [10], to supramolecular quantum approaches, where solute and a few solvent molecules are treated quantum mechanically [10, 11]. Anyway, it seems that, at least to a first approximation, the thermodynamics of such processes is influenced only by static solvent effects [10, 11].

Static solvent effects have been studied for many years, and there are several methods with a progressive increase in the details of the description of the system and, consequently, in the sophistication of the model [12–18]. These effects have been usually treated in the framework of the continuum approach, which considered the solvent as a *bulk* dielectric continuum, polarized by the solute charge distribution. It has been found that this method can model with some accuracy solute–solvent interactions when solvent molecules do not participate in the reaction mechanism [19–22].

In this paper we present an extension to density functional theory (DFT) of one of the most common continuum models, the so called self-consistent reaction field (SCRF) [13, 15, 23, 24], to the study of some organic and inorganic isomerization equilibria. Our attention will be focused on the influence of static solvent effects on the solute electronic distribution, rather than merely on gas-phase/solution structural variations.

2 Continuum model of a solvent effects

The continuum models consider the solvent to be an infinite continuous dielectric medium possessing the macroscopic characteristics (such as dielectric constant) of the pure liquid. The solute is placed into a cavity in the continuum and solute–solvent interactions are treated either classically or quantum mechanically. The solution process thus consists of inserting a solute molecule into a suitable cavity (spending the energy of cavitation for its creation) and *switching on* the interactions with surrounding solvent molecules. The overall change of the Gibbs free energy of solvation, ΔG_{solv}, is generally evaluated as the sum of different contributions [25, 26]:

$$\Delta G_{solv} = G_{cav} + G_{disp-rep} + (G_{enp} - G_{en}) + \Delta G_{vib} \tag{1}$$

where G_{cav} is the cavitation contribution, $G_{disp-rep}$ is the dispersion-repulsion term, G_{enp} includes the SCF total (electron + nuclei) energy of the solute in solution and the solute–solvent polarization terms, both electrostatic and inductive, G_{en} is the SCF total energy of the solute in gas phase and ΔG_{vib} is the change in vibrational free energy (including both zero-point and thermal effects). This latter effect is small and can be neglected safely, in cases involving small amplitude vibrations, such as those reported in Ref. [20]. The factorization of Eq. (1) rests on the assumption that the "hard part" (G_{cav}) and the "soft part" (G_{enp}, G_{en} and $G_{disp-rep}$) can be treated as

independent. This is an oversimplification and must be used with some caution. A detailed discussion on this topic can be found in Ref. [26].

The cavitation term of Eq. (1) can be evaluated from the scaled particle theory (SPT) of fluids [27, 28, 29]. The essence of this theory lies in computing the reversible work required to exclude the solvent molecules (represented by hard spheres) from a region of space in the fluid. The second contribution to the solvation Gibbs free energy, i.e. dispersion-repulsion can be evaluated, under some assumptions, in terms of empirical two-body potentials [30, 31]. Both terms (cavitation and dispersion-repulsion), depending only on the cavity shape, have a negligible effect on the thermodynamics of reaction if the cavity shape can be considered constant [32] and will not be considered further. On the other hand, several attempts to account for the dominant electrostatic contribution, ranging from the simple Born equation [33, 34] to different reaction field (RF) models [13, 15, 23, 24] exist.

A comprehensive review of most common solvent continuum models can be done in terms of classical electrodynamics [35]. As mentioned above, in all the continuum models a solute is considered to occupy a cavity and be surrounded by a linear, isotropic continuum dielectric, having the macroscopic characteristics, such as the dielectric constant, of the pure liquid. The electrostatic potential Φ, generated by the charge distribution ρ of the solute molecule, inside the cavity, must satisfy the Poisson equation:

$$\nabla^2\Phi = -4\pi\rho\,. \tag{2}$$

The boundary conditions of the Poisson equation are determined by the model: the dielectric permitivity. ε, is zero inside the cavity volume (V) and equal to the macroscopic value, ε_0, outside, whereas the molecular charge distribution ρ is completely located inside the cavity. These conditions are summarized as:

$\varepsilon = 1$	inside the cavity
$\varepsilon = \varepsilon_0$	outside the cavity
$\rho = \rho(r)$	inside the cavity
$\rho = 0$	utside the cavity

The boundary conditions so defined are

$$\Phi_i(r) = \Phi_e(r), \tag{3}$$

$$\left(\frac{\partial\Phi}{\partial n}\right)_i = \varepsilon_0\left(\frac{\partial\Phi}{\partial n}\right)_e \tag{4}$$

where $\partial/\partial n$ is the derivative normal to the cavity surface and the subscripts i and e indicate points lying at infinitely small distance from the cavity surface, on its internal or external side, respectively. The general solution of Eq. 2 is

$$\Phi = \int\frac{\rho(r')}{|r'-r|}\mathrm{d}V + \psi \tag{5}$$

where ψ is the contribution due to the charge distribution outside the cavity, and the integral is over the entire volume V of the cavity.

The solute–solvent interaction energy is a function of the solute charge distribution:

$$E_{\mathrm{int}} = -\frac{1}{2}\int\rho\psi\,\mathrm{d}V \tag{6}$$

The evaluation of this energy, which is equal to the inverse of the work of charging the continuum dielectric, and the explicit solution of the Poisson equation depend on the kind of cavity chosen for the solute molecule. In particular, the Poisson equation is separable if the cavity surface constitutes a constant coordinate surface.

If this latter is modeled as a sphere, the ψ can be written (in polar coordinates r, φ, ϑ), as:

$$\psi = \sum_{n=0}^{\infty} \sum_{m=-n}^{n} B_{nm} r^n P_n^m(\cos \vartheta) e^{im\varphi} \tag{7}$$

where P_{nm} are the associated Legendre functions, and B_{nm} are constants to be determined by the above-mentioned boundary conditions. The interaction energy can be written [12], in atomic unit, as:

$$E_{\text{int}} = -\frac{1}{2} \sum_{n=0}^{\infty} \sum_{m=-n}^{n} f_n M_n^m M_n^m e m. \tag{8}$$

where

$$f_n = \frac{(n+1)(\varepsilon - 1)}{n + \varepsilon(n+1)} \frac{1}{a^{2n+1}},$$

$$M_n^m = \int \rho m_n^m \, dV, \quad m_n^m = \left(\frac{4\pi}{2n+1}\right)^{1/2} r^n Y_n^m(\vartheta, \varphi).$$

In the above equation, M_n^m is the expectation value of the charge, dipole and higher moments m_n^m. The superscript m refers to the real component of the n-pole, e.g. x, y, z components of the dipole. The product $f_n M_n^m$ represents the reaction field of the solvent to the M_n^m-pole of the solute. The first term in the expansion (7) is the Born term [33]:

$$E_{\text{int}}^{(1)} = -\frac{1}{2}\left(1 - \frac{1}{\varepsilon}\right)\left(\frac{1}{a}\right) Q^2, \tag{9}$$

where Q is the net charge of the solute. The second term is the Onsager dipolar term [13]:

$$E_{\text{int}}^{(2)} = -\frac{1}{2} \frac{2(\varepsilon - 1)}{(2\varepsilon + 1)} \frac{1}{a^3} \mu^2 = -\frac{1}{2} g(\varepsilon, a) \mu^2. \tag{10}$$

The Born term is, of course, non-vanishing only for a charged solute ($Q \neq 0$). In this case also Eq. (5) must be modified in such a fashion that the moments are invariant with respect to the position [24, 36]. This necessitates separating the positive and negative parts of the moments and for a net negative system multiplying the dipole terms by

$$f_m^- = \frac{n + Q}{n}$$

and for a net positive solute

$$f_m^+ = \frac{n}{n + Q}$$

with n being the total number of electrons inside the cavity and Q being the net charge in the same region. It must be pointed out that E_{int} is actually the sum of

electrostatic interaction between the solute and the dielectric plus the energy needed to polarize the dielectric. For instance, in the Onsager model the total energy of a solute in the solvent cavity can be expressed as:

$$E_{tot} = E^0_{RF} + E_{el} + E_{polarizing} = E^0_{RF} - g\mu\mu + \tfrac{1}{2} g\mu\mu = E^{(0)}_{RF} - \tfrac{1}{2} g\mu\mu. \quad (11)$$

where E^0_{RF} is the total energy of the solute in the presence of the RF, but without including the interaction with it, and the last term ($-\frac{1}{2} g\,\mu\mu$) is the E_{int} of Eq. (10). Of course, E^0_{RF} is greater than that in gas phase ($E^0_{(gas)}$), i.e. the solute is destabilized by an external field (the RF).

Higher expansions of Eq. (12) (including quadrupole, hexapole, etc.) can be considered, especially in studying interaction for highly symmetric molecules with dipole moments equal to zero, such as the formamide dimer or the methane molecule. A similar approach has been developed for more complex ellipsoidal cavities [37, 38].

The situation is more involved if a more detailed cavity is introduced, since the solution of the Poisson Eq. (2) is no longer analytical and numerical iterative procedure must be introduced [1, 16]. Very recently an alternative approach, resting on the Green function method, has been introduced to solve analytically the Poisson equation [18]. In this approach a strong dielectric medium (such as water, $\varepsilon = 80$) is represented as an infinitely strong dielectric ($\varepsilon = \infty$), i.e. a conductor.

From a more technical point of view, the RF, especially in the form appearing in Eq. (8), can be treated as a static external electric field, i.e. as an additional term to the molecular hamiltonian. In particular, this approach in the dipolar version (the Onsager model, Eq. (10) leads to a straightforward introduction of the RF in the Hamiltonian matrix [24, 39].

Some further remarks on the use of SCRF must be added. First of all, as mentioned above, the Onsager model, the simplest SCRF approach, is satisfactory in the case of comparatively rigid molecules bearing large dipole moments, whereas it fails in those cases in which the dipole moment is small or zero and higher moments dominate the solute–solvent interaction. Moreover in the study of rigid molecules, such as formamide or 2-pyridone, it has been found that the presence of the solvent field has a negligible effect on the geometry of the solute molecule [11, 20]. This allows us to evaluate solvent effects via single point energy corrections on the gas-phase relaxed geometries.

3 Case studies

We have analyzed the influence of bulk water solvent on three examples which show different relevance of the contribution of Eq. (11). Preliminary results have been reported [39]. The first two are the tautomerization reactions of formamide in formamidic acid (F/FA) and 2-pyridone in 2-hydroxypyridine (2Py/2Hy) (Fig. 1), while the third is the linkage isomerization of pentaamminenitrito cobalt(III) ion, $[Co(NH_3)_5ONO]^{2+}$ (hereafter CoONO), to pentamminenitro cobalt(III) ion, $[Co(NH_3)_5NO_2]^{2+}$ (hereafter $CoNO_2$, see Fig. 2). The first two systems have been chosen both for their intrinsic interest and because they are well characterized from experimental [40–44] and theoretical [11, 20, 21, 45–49] points of view. As concerns the 2-pyridone the relative stability of the two tautomers has been discussed for several years and many experimental studies have been devoted to the study of this problem [40–42]. The main conclusion is that the 2Hy is favored in the gas-phase or in non-polar solvents, whereas the 2Py predominates in polar solvents

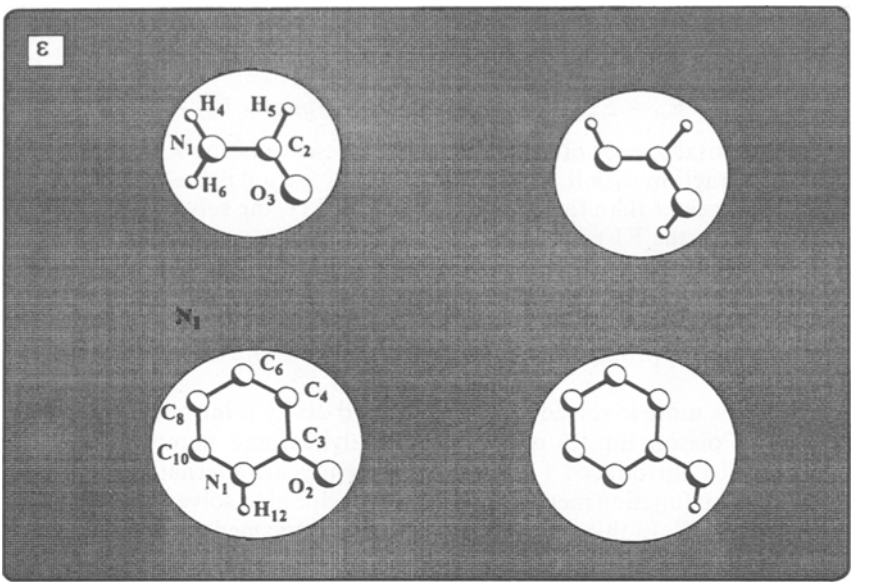

Fig. 1. *Up*: formamide (*left*) and its formamidic acid tautomer (right); *Down*: 2-pyridone (*left*) and its 2-hydroxypyridine tautomer (*right*)

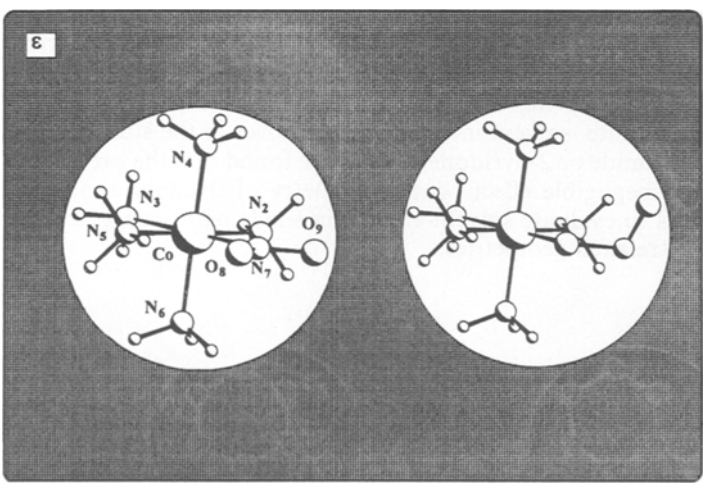

Fig. 2. The structure of the two Co(III) complexes: pentaamminenitrocobalt(III) ion (*left*) and the pentaamminenitrito-cobalt(III) ion (*right*)

or in aqueous solutions [41]. These results are supported by a number of theoretical studies [11, 20, 21]. Also the interconversion between the two Co(III) isomers has been the object of many investigations, being the first case of such phenomena discovered [50], and it is considered in all inorganic chemistry textbooks [51] as

the prototype of this class of reactions. A wealth of experimental data has been gathered on thermally [52–55] and photochemically activated [56–58] processes, both in the solid state and in solution. Experimental findings in solution show that isomerization of the nitrito complexes to the corresponding nitro compounds is complete in solution and has a first-order rate constant for rearrangement. The results [55, 59] strongly suggest that metal to oxygen bond cleavage does not occur during the isomerization and establish that the NO_2^- ion never leaves the influence of the coordination sphere. Furthermore both spontaneous and base-catalyzed processes are intramolecular. As a consequence, nonspecific solute–solvent interactions play a relevant role in the thermodynamics of the reaction, whereas specific interactions should have a significant effect on the kinetics, modifying the reaction path.

4 Computational methods

All the electronic calculations were carried out using the ADF package [60, 61]. This is a LCAO density functional program system, which uses a numerical integration algorithm [62] for the evaluation of the matrix elements appearing in the secular equation. The molecular orbitals were expanded in an uncontracted double-ζ STO basis set [63]. One polarization function was added on H and first-row atoms, while the cores (C,N,O 1*s*; Co 1*s*-2*p*) have been kept frozen. A set of auxiliary *s*, *p*, *d*, *f* and *g* STO functions [64], centered on all non-H nuclei, was used to fit the molecular density and to generate the Coulomb and exchange potential accurately in each SCF cycle. Bond energies were evaluated by the generalized transition state method [65]. The calculations performed in the local spin density (LDA) approximation employ the Vosko, Wilk and Nusair parametrization [66] for the correlation energy of the homogeneous gas. Nonlocal density gradient type correlations were included using the functional of Becke for exchange [67], and Perdew for correction [68]. This kind of calculation will be labeled "GC-LDA". All the molecules were fully optimized both at LDA and GC-LDA level, using an algorithm, based on numerical integration, which allows to evaluate energy gradients analytically [69].

The SCRF model has been introduced [39] in the ADF package in the Onsager version, i.e. truncating the expansion of Eq. (7) to the dipole level. This model contains as an adjustable parameter the radius (a_0) of the spherical cavity embedding the solute. This parameter can be computed by the molecular volume in several ways, ranging from simple geometrical considerations to solvent accessible volume. Here, following the recipe proposed by Frisch and coworkers [20], the radius was computed from the isodensity surface at 0.001 au and next augmented by 0.5 Å to account for the nearest approach of solvent molecule. The computed cavity radius, constant for the two tautomeric forms, was 3.2 Å for a formamide, 3.8 Å for the pyridone and 4.2 Å for the Co complexes. The assumed value for the dielectric constant was 78.35, which is the standard value for water.

5 Gas-phase structures

The gas-phase optimized bond lengths and valence angles of the formamide and formamidic acid are reported in Table 1. Experimental data are only available for

Table 1. Optimized DFT bond lengths (Å) and angles (degrees) of the two energy minima characterizing the tautomerization of the formamide in the gas phase. At GC-LDA level, the two ammino hydrogens (H_4 and H_6) are out of the N_1–C_2–O_3 plane of about 6°

	Formamide						Formamidic acid			
	HF[a]	MP2[a]	LDA	GC-LDA[b]	GC-LDA	exp.[c]	HF[a]	MP2[a]	LDA	GC-LDA
N_1–H_4	0.991	1.005	1.024	1.021	1.024	1.002	1.001	1.016	1.032	1.034
N_1–H_6	0.994	1.002	1.028	1.024	1.028	1.002	2.282	2.294	2.256	2.305
N_1–C_2	1.348	1.360	1.345	1.369	1.363	1.360	1.246	1.273	1.259	1.268
C_2–O_3	1.193	1.223	1.214	1.227	1.223	1.219	1.338	1.349	1.336	1.358
C_2–H_5	1.092	1.100	1.122	1.125	1.120	1.098	1.081	1.087	1.103	1.101
O_3–H_6							0.948	0.971	0.999	0.997
H_4–N_1–C_2	121.6	121.7	121.1	121.3	121.2	118.8	57.5	56.8	55.7	55.0
H_6–N_1–C_2	119.1	118.8	119.1	119.6	119.3	121.4	111.8	110.0	112.2	111.3
O_3–C_2–N_1	124.9	124.8	124.7	124.9	125.0	124.5	122.6	121.7	121.5	122.1
H_5–C_2–N_1	112.8	112.1	112.4	111.9	112.3	112.7	126.8	128.1	128.3	127.9

[a] HF/6-31G** and MP2/6-31G** computations, Ref. [20]; [b] Ref. [70]; [c] Ref. [43].

the formamide monomer [44] and are included for comparison purposes, together with previously published theoretical data [20, 70]. The minima were characterized by computing vibrational frequencies, both at LDA and GC-LDA levels. As expected the GC-LDA geometrical parameters of formamide are in better agreement with experimental data than LDA values and are close to the MP2 results. The only significant differences are in those bonds involving H atoms, that are systematically overestimated by about 0.02 Å. On the other hand, the bond distances of the formamidic acid computed at the GC-LDA level are slightly different with respect to MP2 results, the greater difference being of 0.01 Å for the CO bond. Also in this case the X–H bonds seem to be overestimated. All the bond lengths change as the tautomerization proceeds. In particular at the GC-LDA level, in the formamide monomer the N_1C_2 bond length is reduced from 1.363 to 1.268 Å, while the CO distance increases from 1.223 to 1.358 Å, on going from formamide to formamidic acid. This is consistent with the breaking of the CO double bond and the corresponding formation of the CN double bond. It is noteworthy that formamide, both at LDA and GC-LDA levels, is not planar, with the hydrogens of the amino group about 6° (at GC-LDA level) out of the NCO plane. This bent molecule is consistent with some recent X-ray structures of amino groups [71, 72]. The optimized planar structure is 2.3 kcal/mol higher in energy, but it is a first-order saddle point, with one imaginary frequency ($242i\ cm^{-1}$), corresponding to the out-of-plane motion of the amino group.

The LDA and GC-LDA geometrical parameters for 2-pyridone and 2-hydroxypyridine are reported in Table 2. The minimum points on the potential energy surface were characterized by computing vibrational frequencies, both at LDA and GC-LDA level. LDA bond lengths are uniformly longer than the corresponding HF values. The inclusion of nonlocal effects further increases all the bond distances, which are now close to MP2 values and in good agreement with the available X-ray data [73]. This trend indicates that electron correlation plays a relevant role in determining the structure of these molecules. As mentioned for the formamide, the X–H bonds are systematically overestimated. The geometrical parameters reflect the tautomerization mechanism. At the GC-LDA level, the CO bond length increases from 1.231 to 1.336 Å, passing from 2-pyridone to 2-hydroxypyridine. On the other hand, ring bond lengths reflect the rearrangement of the electronic distribution, changing from a nonaromatic structure (2-pyridone), with localized double bonds (C_4C_6 and C_8C_{10} bonds), to an aromatic structure with all bonds roughly equal. Of course, both molecules are planar, with C_s symmetry.

Table 3 collects LDA optimized geometrical parameters of nitrito, $[Co(NH_3)_5ONO]^{2+}$, and nitro, $[Co(NH_3)_5NO_2]^{2+}$, Co(III) complexes, together with the available experimental data [54, 74]. The agreement between computed and experimental data is good, especially as regards the metal-amino ligand distances, which differ on average by about 0.02 Å with respect to experimental data. On the contrary, both nitrito and nitro distance are too short in comparison with X-ray values (1.88 vs. 1.92 Å for the nitro complex and 1.87 vs. 1.93 Å for the nitrito complex), but it is well known [69, 75] that the LDA is a relatively poor approximation in modelling weak metal–ligand interactions, underestimating the metal ligand distances by about 0.05 Å. Moreover in the case of nitrito complexes the available X-ray data are not so reliable, due to positional disorder, which leads to a very short N–O distance [54].

Table 2. Optimized DFT bond lengths (Å) and angles (degrees) of the two energy minima characterizing the tautomerization of the 2-pyridone in the gas phase

	2-Pyridone					2-Hydroxypyridine			
	HF[a]	MP2[a]	LDA	GC-LDA	exp.[b]	HF[a]	MP2[a]	LDA	GC-LDA
N_1–C_2	1.383	1.404	1.402	1.405	1.401	1.308	1.331	1.320	1.331
C_2–O_3	1.203	1.234	1.222	1.231	1.236	1.335	1.385	1.336	1.359
C_2–C_4	1.457	1.449	1.435	1.453	1.444	1.396	1.399	1.391	1.404
C_4–C_6	1.343	1.367	1.356	1.367	1.334	1.372	1.386	1.375	1.388
C_6–C_8	1.438	1.422	1.407	1.422	1.421	1.395	1.398	1.387	1.400
C_8–C_{10}	1.339	1.363	1.358	1.369	1.371	1.374	1.388	1.380	1.391
N_1–H_{12}	0.996	1.011	1.020	1.038					
O_3–H_{12}						0.946	0.969	0.977	0.997
N_1–C_2–O_3	120.49	120.38	120.06	120.25	121.3	117.75	117.38	118.11	117.07
N_1–C_2–C_4	113.69	112.55	112.65	112.42	112.7	123.98	124.29	123.63	123.81
C_2–C_4–C_6	121.12	122.05	121.86	122.07	122.3	117.24	117.58	117.45	117.33
C_4–C_6–C_8	121.51	121.22	121.45	121.43	122.2	119.71	119.30	119.67	119.69
C_6–C_8–C_{10}	121.51	121.22	118.04	118.19	122.2	117.53	118.32	118.11	118.05
H_{12}–N_1–C_2	114.8	113.7	113.9	114.05				104.34	104.35

[a] HF/6-31G** and MP2/6-31G**, Ref. [20].
[b] Solid State, Ref. [73].

Table 3. Optimized DFT bond lengths (Å) and angles (degrees) of the two energy minima characterizing the pentaamminenitrocobalt(II) isomerization in the gas phase

	$[Co(NH_3)_5NO_2]^{2+}$ [a]		$[Co(NH_3)_5ONO]^{2+}$	
	LDA[b]	exp.[c]	LDA[b]	exp.[d]
$Co-N_7$	1.883	1.921		
$Co-N_2$	1.931	1.985	1.933	1.913
$Co-N_3$	2.002	1.985	1.978	1.948
$Co-N_4$	1.936	1.985	1.928	1.952
$Co-O_8$			1.871	1.927
N_7-O_8	1.216	1.161	1.389	1.244
N_7-O_9	1.216	1.161	1.178	1.037
N–H	1.043		1.043	1.070
O_8-N_7-Co	117.20	123.0	98.47	131.3
$O_9-N_7-O_8$	125.60	113.9	112.11	125.3
H–N–Co	114.89		117.39	

[a] Symmetry Cs; [b] Ref. [39]; [c] Ref. [74]; [d] Ref. [54].

Table 4. Dipole moments and Mulliken charges for the formamide tautomers, in the gas phase and in aqueous solution

Atom	Formamide				Formamidic acid			
	LDA		GC-LDA		LDA		GC-LDA	
	Gas phase	Solution	Gas phase	Solution	Gas phase	Solution	Gas phase	Solution
N_1	−0.621	−0.619	−0.633	−0.631	−0.634	−0.636	−0.643	−0.647
C_2	0.735	0.730	0.779	0.774	0.679	0.679	0.708	0.709
O_3	−0.695	−0.714	−0.711	−0.731	−0.721	−0.721	−0.737	−0.737
H_4	0.278	0.294	0.274	0.289	0.175	0.177	0.176	0.178
H_5	0.052	0.055	0.042	0.047	0.118	0.122	0.105	0.109
H_6	0.251	0.254	0.250	0.242	0.382	0.378	0.392	0.388
Dipole moments (D)								
μ	3.574	4.304	3.892	4.274	1.059	1.141	1.047	1.126

6 Solvent effects on electronic wave functions

The electronic distribution of formamidic acid is only slightly influenced by the presence of a dielectric medium, whereas larger effects are found for the more polar keto form (see Table 4). The overall solvent effects are well reflected by the values of the dipole moments. In fact, the dipole moments for isolated formamide is 3.89 D at the GC-LDA level, while in aqueous solution it rises to 4.27 D. For formamidic acid the dipole essentially does not change being 1.047 and 1.126 D at the GC-LDA level in the gas-phase and aqueous solution, respectively.

The electronic distribution of 2-pyridone is strongly altered by the presence of water solvent, while the distribution of the less polar 2-hydroxypyridine suffers

Table 5. Dipole moments and Mulliken charges for Py and Hy in the gas phase and in aqueous solution

Atom	2-Pyridone				2-Hydroxypyridine			
	LDA		GC-LDA		LDA		GC-LDA	
	Gas phase	Solution	Gas phase	Solution	Gas phase	Solution	Gas phase	Solution
N_1	−0.621	−0.620	−0.644	−0.644	−0.653	−0.656	−0.677	−0.680
C_2	0.726	0.717	0.753	0.745	0.709	0.706	0.724	0.721
O_3	−0.713	−0.738	−0.725	−0.751	−0.715	−0.717	−0.729	−0.731
C_4	−0.287	−0.293	−0.278	−0.286	−0.227	−0.227	−0.218	−0.219
C_6	−0.133	−0.129	−0.121	−0.117	−0.128	−0.127	−0.115	−0.113
C_8	−0.230	−0.224	−0.225	−0.218	−0.228	−0.226	−0.220	−0.218
C_{10}	0.187	0.190	0.213	0.217	0.135	0.134	0.166	0.166
Dipole moments (D)								
μ	4.169	5.354	4.122	5.325	1.116	1.433	1.178	1.516

Table 6. Dipole moments and Mulliken charges for pentaamminenitrocobalt(II) and pentaamminenitritocobalt(II) in the gas phase and in aqueous solution. The values refer to fully optimized LDA geometry

Atom	$[Co(NH_3)_5NO_2]^{2+}$				$[Co(NH_3)_5ONO]^{2+}$			
	LDA		GC-LDA		LDA		GC-LDA	
	Gas phase	Solution	Gas phase	Solution	Gas phase	Solution	Gas phase	Solution
Co	1.029	1.039	1.041	1.122	1.051	1.035	1.113	1.122
N_7	0.534	0.517	0.535	0.522	0.431	0.415	0.436	0.423
N_2	−0.848	−0.849	−0.848	−0.854	−0.825	−0.838	−0.856	−0.856
N_3	−0.880	−0.889	−0.879	−0.903	−0.858	−0.876	−0.881	−0.890
N_4	−0.839	−0.852	−0.838	−0.861	−0.835	−0.841	−0.850	−0.853
O_8	−0.432	−0.465	−0.435	−0.478	−0.550	−0.531	−0.544	−0.556
O_9	−0.432	−0.465	−0.435	−0.478	−0.316	−0.393	−0.335	−0.399
Dipole moments (D)								
μ	7.254	9.792	7.349	9.644	6.672	10.360	7.085	10.198

no significant modifications (see Table 2). For instance, the dipole moment of 2-pyridone is 4.12 D in gas phase (GC-LDA level) and it rises to 5.33 D in aqueous solution, while the corresponding values for 2-hydroxypyridine are 1.18 and 1.52 D (see Table 5).

Also in the case of the Co(II) complexes there are significant modifications in the electronic distribution on passing from gas phase to aqueous solution, in particular as regards the nitrito complex (Table 6). In fact for the CoONO isomer the dipole moments change from 7.09 D in gas phase to 10.20 D in aqueous solution. Also the electronic distribution of the nitrito complex is altered by solvent interactions, but less drastically, the dipole moments being 7.35 and 9.62 D in gas phase and aqueous solution, respectively.

Table 7. Endothermicity for the considered tautomerization reactions in the gas phase and energy contribution to the solvation energy, computed at the GC-LDA level. Energy values (in kcal/mol) refer to gas-phase optimized geometries

	Gas-phase				Solution		
	MP2[a]	CI[b]	LDA[c]	GC-LDA	ΔE^0_{RF}	E_{int}	ΔE_{tot}
F	0.0	0.0	0.0	0.0	0.7	− 6.1	− 5.4
FA	12.5	11.8	10.7	11.8	12.1	− 0.4	11.7
Py	3.8	0.6	1.2	0.5	0.8	− 7.2	− 6.4
Hy	0.0	0.0	0.0	0.0	0.2	− 0.9	− 0.7
Co–NO_2			3.9	9.9	10.4	− 29.0	− 18.6
Co–ONO			0.0	0.0	26.7	− 40.2	− 13.5

[a] MP2/6-31G**, Ref. [11]; [b] QCISD/6-31G** on HF/6-31G** geometries, Ref. [20].
[c] Ref. [39].

7 Solvent effects on reaction energetics

Table 7 reports the endothermicities for all the considered isomerizations, together with the different contribution to the ΔE_{tot} in solution (Eq. (11)) at the GC-LDA level, with respect to the most stable compound in the gas phase. LDA results are taken from Ref. 39. All the computations in solution refer to the gas phase geometries.

Let us start the discussion with the F/FA couple. The LDA computations indicate an endothermicity in the gas phase of 10.7 kcal/mol that is lower than all ab initio results. On the other hand the more reliable GC-LDA value (11.8 kcal/mol) is in close agreement with the experimental estimate, 11 ± 4 kcal/mol, and it is equal to the best ab initio (QCISD) results [20]. The reaction field of the water solvent plays a non negligible role in the tautomerization reaction. In fact the endothermicity of the keto-enol transformation is enhanced by the solvent effect to 5.9 kcal/mol and 5.3 kcal/mol at the LDA and GC-LDA levels, respectively, as can be easily computed from data reported in Table 7. The corresponding ab initio value is 4.4 kcal/mol at the HF/6-31G** level [76]. This behavior can be understood by examining all the different contributions. As mentioned above, the external field, generated by the solvent, destabilizes the solute, leading to an increase of its internal energy (ΔE^0_{RF} of Table 7). In particular F and FA are slightly destabilized by the RF, their energies rising of 0.7 and 0.3 kcal/mol. On the contrary F, due to its higher dipole moment, suffers much more the solvent interactions with respect to FA (− 6.1 vs. − 0.4 kcal/mol, respectively). The net effect is a stabilization with respect to the gas phase of 5.4 kcal/mol for the F and only 0.1 kcal/mol for the FA. So the solvent increases the energy gap between the two tautomeric forms (here F), stabilizing the form with the highest dipole moment. The solvent has a different effect on the 2Py/2Hy tautomerization. Both LDA and GC-LDA computations, without the solvent contribution, indicate the 2-pyridone as the less stable molecule (1.2 and 0.5 kcal/mol with respect to 2-hydroxypyridine). The LDA result is close to HF computations [11] (1.0 kcal/mol) carried out using a large basis set (6-31G**), while GC-LDA is comparable with the sophisticated QCISD approach [20] (0.6 kcal/mol). The lower stability of the lactam form is in agreement with gas-phase experimental

findings [40] (1 kcal/mol). It is noteworthy that the MP2 method, which gives reliable structures, overestimates this value (3.8 kcal/mol).

The solvent reaction field reverses the relative stability of the two tautomeric forms. In fact, 2-pyridone is stabilized by solvent interactions with respect to 2-hydroxypyridine and the endothermicity for the tautomerization reaction is, consequently, enhanced to 5.8 kcal/mol at GC-LDA level. An analysis of the energy contributions, shows a behavior near to that observed for formamide and formamidic acid.In fact both tautomers are destabilized by a roughly equal amount (0.3 and 0.2 kcal/mol for 2Py and 2Hy, respectively). but the two molecules interact in different ways with the solvent, the interaction energy being -7.2 kcal/mol for 2Py and -0.9 kcal/mol for 2Hy. The total effects is a net stabilization of both tautomers, but 2Py is much more stabilized than 2Hy (6.4 vs. 0.7 kcal/mol).

Our gas-phase results indicate the nitrito complex as the most stable isomer by 3.3 and 9.9 kcal/mol at the LDA and GC-LDA levels, respectively. This is in contrast with experimental findings in solution [59]. The inclusion of the solvent reaction field has a determining role on the relative stability of the two isomers. In fact the computed endothermicity in aqueous solution is 5.1 kcal/mol at the GC-LDA level in favor of the nitro compounds (Table 6). This result is in relatively good agreement with an experimental estimate that indicates a value not lower than 2 kcal/mol [59]. At first sight the new order of stability, even though in agreement with the experimental trend, can be surprising since the molecule with the larger dipole moment in solution (nitrito isomer, see Table 7) is less stable. This behavior can be ascribed to an electronic stabilization due to the solvent electric field. In fact the difference between the electronic energy in vacuo and in the presence of the electric field generated by the solvent (ΔE^0_{RF}) is 10.4 kcal/mol for the nitrito isomer, while it amounts to only 26.7 kcal/mol for the nitro complex (at GC-LDA level). On the contrary the solvent reaction field interacts more strongly with the nitrito complex ($E_{int} = -40.2$ kcal/mol) than with the nitro one ($E_{int} = -29.0$ kcal/mol). The net effect is a stabilization of $CoNO_2$ with respect to CoONO. This behavior, much more pronounced than in organic molecules, could be ascribed to a larger electronic rearrangement of the nitrito compounds, which leads a very large destabilization not present in the case of nitro isomer, and whose value overcomes the stabilization contribution due to solute–solvent interactions. These last results suggest that charges derived from electronic wavefunctions in the gas phase can be used safely in computing the electrostatic contribution to the solvation free energy of organic compounds [77], whereas some caution is needed for transition metal complexes.

Conclusion

We have reported the results of a study of some of the most common tautomerization in organic and inorganic chemistry. In particular, we pointed out the influence of non-specific solute–solvent interactions on the thermodynamics of such reactions in the framework of DFT. These interactions can be well modeled by a reaction field model. Moreover our results suggest that in the case of the studied coordination compound, and probably in coordination compounds in general, it might be essential to use, as in the presented study, a self-consistent version which is able to take into account the electronic rearrangement due to field effects in solution.

Acknowledgements. This work has been financially supported by Italian CNR, CT12, and by MURST. CISIT of University of Basilicata is also acknolwedged for computational support. One of us (F.L.) thanks NSERC of Canada for a grant, received during a summer stay at the Department of Chemistry of University of Calgary (Alb.), and Prof. T. Ziegler for helpful discussions and warm hospitality.

References

1. Aguilar MA, Olivares FJ, Tomasi J (1993) J Chem Phys 98:7375
2. Kim HJ, Hynes JT (1990) J Chem Phys 93:5194
3. Tucker SC, Truhlar DG (1990) J Am Chem Soc 112:3347
4. Basilevsky MV, Chudinov GE (1991) Chem Phys 157:327
5. Marcus RA (1992) J Phys Chem 96:1753
6. Hockney RW, Eastwood JW (1980) Computer simulation using particles. McGraw-Hill, New York
7. Ciccotti G, Frenkel D, McDonald IR (eds) (1988) Simulation of liquids and solids. Clarendon, New York
8. van Gunsteren WF, Weiner PK (1989) Computer simulation of biomolecular systems, Vol I. ESCOM, Leiden
9. Cristinziano PL, Lelj F, Amodeo P, Barone V (1987) Chem Phys Lett 401:1235
10. Warshel A (1991) Computer modeling of chemical reactions in enzymes and solutions. Wiley, New York; Luzhkov V, Warshel A (1992) J Comp Chem 13:199; Hwang JK, King G, Creighton S, Warshel A (1988) J Am Chem Soc 110:5297
11. Barone V, Adamo C (1994) J Comp Chem 15:395
12. Kirkwood JG (1934) J Chem Phys 2:351
13. Onsager L (1936) J Am Chem Soc 58:1468
14. Rinaldi D, Rivail JL (1973) Theor Chim Acta 32:57
15. Tapia O, Goscinski O (1975) Mol Phys 29:1653
16. Miertus S, Scrocco E, Tomasi J (1981) Chem Phys 55:117
17. Cramer CJ, Truhlar DG (1991) J Am Chem Soc 113:8305
18. Klamt A, Schuurmann G (1993) J Chem Soc Perkin Trans 2:799
19. Karelson M, Tamm T, Zerner MC (1993) J Phys Chem 97:11901
20. Wong MW, Wiberg KB, Frisch MJ (1992) J Am Chem Soc 114:1645
21. Szafran M, Karelson MM, Katritzky AR, Koput J, Zerner MC (1993) J Comput Chem 14:371
22. Young PE, Hillier IH (1993) Chem Phys Lett 215:405
23. Tapia O (1991) J Mol Struct (THEOCHEM) 226:59
24. Wong MW, Wiberg KB, Frisch MJ (1991) J Chem Phys 95:8991
25. Eley DD (1944) Trans Faraday Soc 40:184
26. Ben-Naim A (1987) Solvation thermodynamics. Plenum, New York
27. Hill TL (1958) J Chem Phys 28:1179
28. Reiss H (1966) Adv Chem Phys 9:1
29. Pierotti RA (1976) Chem Rev 76:717
30. Floris FM, Tomasi J (1989) J Comp Chem 10:616
31. Floris FM, Tomasi J, Pascual Ahuir JL (1991) J Comp Chem 12:784
32. Adamo C, Barone V, Loison S, Minichino C (1993) J Chem Soc Perkin Trans 2:697
33. Born M (1920) Z Phys 1:45
34. Rashin AA, Honig B (1985) J Phys Chem 89:5588
35. Jackson JD (1975) Classical electrodynamics. Wiley, New York
36. Karelson MM, Zerner MC (1992) J Phys Chem 96:6949
37. Rivail JL, Terryn B (1982) J Chim Phys 79:1
38. Rinaldi D, Ruiz-Lopez MF, Rivail JL (1983) J Chem Phys 78:834
39. Adamo C, Lelj F (1994) Chem Phys Lett, in press
40. Beak P, Covington JB, Smith SG (1976) J Am Chem Soc 98:186
41. Beak P (1977) Acc Chem Res 10:1866 and refs. therein
42. Beak P, Covington JB, Smith SG, White JM, Ziegler JM (1980) J Org Chem 45:1354
43. Hirota E, Sugisaki R, Jorgen C, Sorensen GO (1974) J Mol Spectr 49:251

44. Brown RD, Godfrey PD, Kleibomer BJ (1987) J Mol Struct 124:34
45. Moreno M, Miller WH (1990) Chem Phys Lett 171:475
46. Parchment OG, Burton NA, Hillier IH (1993) Chem Phys Lett 203:46
47. Wojcik MJ, Hirakawa AY, Tsuboi M (1986) Int J Quantum Chem QBS 13:133
48. Del Re G, Adamo C (1991) J Phys Chem 95:721
49. Wiberg KB, Breneman CM (1992) J Am Chem Soc 114:831
50. Jorgensen SM (1890) J Prakt Chem 41:454
51. Purcell KF, Kotz JC (1985) Inorganic chemistry. Holt Saunders, London
52. Murmann RK, Taube H (1956) J Am Chem Soc 78:4886
53. Pearson RG, Henry PM, Bergmann JG, Basolo F (1956) J Am Chem Soc 78:5920
54. Grenthe I, Nordin E (1979) Inorg Chem 18:1869
55. Jackson WG, Lawrance GA, Lay PA, Sargeson AM (1980) Inorg Chem 19:904
56. Basolo F, Hammaker GS (1962) Inorg Chem 1:1
57. Balzani V, Ballardini R, Sabbatini N, Moggi L (1968) Inorg Chem 7:1398
58. Mares M Palmer DA, Kelm H (1978) Inorg Chim Acta 27:153
59. Jackson WG, Lawrance GA, Lay PA, Sargeson AM (1982) Aust J Chem 25:1561
60. A modified version of Amsterdam Density Functional System (ADF), Department of Theoretical Chemistry, Vrije Universiteit, De Boelelaan 1083, 1081 HV Amsterdam, The Netherlands
61. Baerends EJ, Ros P (1978) Int J Quantum Chem Symp 12:169
62. Boerringter PM, te Velde G, Baerends EJ (1988) Int J Quantum Chem 33:87
63. Snijders JG, Vernooijs P, Baerends EJ (1982) At Data Nucl Data Tables 26:483 Vernooijs P, Snijders JG, Baerends EJ (1981) Internal Report, Vrije Universiteit, Amsterdam
64. Krijn J, Baerends EJ (1984) Internal Report, Vrije Universiteit, Amsterdam
65. Ziegler T, Rauk A (1977) Theoret Chim Acta 46:1
66. Vosko SH, Wilk L, Nusair M (1980) J Can Phys 58:55
67. Becke AD (1988) Phys Rev A 38:3098
68. Perdew JP (1986) Phys Rev B 33:8822
69. Versluis L, Ziegler T (1988) J Chem Phys 88:322
70. Sim F, St-Amant A, Papai I, Salahub DR (1992) J Am Chem Soc 114:4391
71. Bennet AJ, Wang QP, Slebockatilk H, Somayaji V, Brown RS (1990) J Am Chem Soc 112:6383
72. Shea KJ, Lease TG, Ziller JW (1990) J Am Chem Soc 112:8627
73. Penfold B (1953) Acta Crystallogr 6:591
74. Cotton FA, Edwards WT (1968) Acta Crystallogr Sect. B 24:474
75. Ziegler T (1991) Chem Rev 91:651
76. Barone V, Adamo C, Minichino C (1994) J Mol Struct (THEOCHEM), accepted
77. Montagnani R, Tomasi J (1993) J Mol Struct (THEOCHEM) 279:131